Spin-Orbit Coupling Controlled $J = 3/2$ Electronic Ground State in $5d^3$ Oxides

A. E. Taylor,[1] S. Calder,[1] R. Morrow,[2] H. L. Feng,[3] M. H. Upton,[4] M. D. Lumsden,[1] K. Yamaura,[3]
P. M. Woodward,[2] and A. D. Christianson[1,5,*]

[1]*Quantum Condensed Matter Division, Oak Ridge National Laboratory, Oak Ridge, Tennessee 37831, USA*
[2]*Department of Chemistry, The Ohio State University, Columbus, Ohio 43210-1185, USA*
[3]*Research Center for Functional Materials, National Institute for Materials Science,
1-1 Namiki, Tsukuba, Ibaraki 305-0044, Japan*
[4]*Advanced Photon Source, Argonne National Laboratory, Argonne, Illinois 60439, USA*
[5]*Department of Physics and Astronomy, The University of Tennessee, Knoxville, Tennessee 37996, USA*
(Received 10 November 2016; published 16 May 2017)

Entanglement of spin and orbital degrees of freedom drives the formation of novel quantum and topological physical states. Here we report resonant inelastic x-ray scattering measurements of the transition metal oxides Ca_3LiOsO_6 and Ba_2YOsO_6, which reveals a dramatic spitting of the t_{2g} manifold. We invoke an intermediate coupling approach that incorporates both spin-orbit coupling and electron-electron interactions on an even footing and reveal that the ground state of $5d^3$-based compounds, which has remained elusive in previously applied models, is a novel spin-orbit entangled $J = 3/2$ electronic ground state. This work reveals the hidden diversity of spin-orbit controlled ground states in $5d$ systems and introduces a new arena in the search for spin-orbit controlled phases of matter.

The electronic ground state adopted by an ion is a fundamental determinant of manifested physical properties. Recently, the importance of spin-orbit coupling (SOC) in creating the electronic ground state in $5d$-based compounds has come to the fore and revealed novel routes to a host of unconventional physical states including quantum spin liquids, Weyl semimetals, and axion insulators [1,2]. As a result, major experimental and theoretical efforts have been undertaken seeking novel spin-orbit physics in various $5d$ systems, and the influence of SOC has now been observed in the macroscopic properties of numerous systems. However, beyond the $J_{eff} = 1/2$ case, such as that found in Sr_2IrO_4 [3]—which is a single-hole state that applies only to idealized $5d^5$ ions in cubic materials—questions abound concerning the nature of the electronic ground states which govern $5d$ ion interactions.

In this context $5d^3$ materials present a particularly intriguing puzzle, because octahedral d^3 configurations are expected to be orbitally quenched $S = 3/2$ states—in which case SOC enters only as a third order perturbation [4]—yet there is clear experimental evidence that SOC influences the magnetic properties in $5d^3$ transition metal oxides (TMOs). This includes the observations of large, SOC-induced spin gaps in their magnetic excitation spectra [5–7] and x-ray absorption branching ratios which deviate from $BR = I_{L3}/I_{L2} = 2$ [8,9]. Despite this, no description beyond the $S = 3/2$ state has been established. The emergent phenomena in $4d^3$ and $5d^3$ systems, such as incredibly high magnetic transition temperatures [10–13], Slater insulators [14], and possible Mott insulators [15], are therefore poorly understood.

We selected $5d^3$ TMOS Ca_3LiOsO_6 and Ba_2YOsO_6 as model systems in which to investigate the influence of spin-orbit coupling on the electronic ground states via resonant inelastic x-ray scattering (RIXS) measurements on polycrystalline samples. Both materials have relatively high magnetic ordering temperatures, $T_N = 117$ and 67 K, respectively, despite large separation of nearest-neighbor Os ions of 5.4–5.9 Å [5,10,16]. The relative isolation of Os-O octahedra allows us to unambiguously access the ground state, because only extended superexchange interactions are present. Stronger, close-range interactions can mask the effective single-ion levels we wish to observe [17]. This is likely the reason that the SOC splitting of levels was not observed in the recent RIXS measurement of $5d^3$ $Cd_2Os_2O_7$ [7] and $NaOsO_3$ [18]. In Ca_3LiOsO_6 the oxygen octahedra surrounding Os^{5+} ions are very close to ideal, despite the overall noncubic symmetry—hexagonal $R\bar{3}c$ [10] and consequently Ca_3LiOsO_6 serves as a test if considerations beyond the local octahedral environment are important. As previously reported [5], we find that Ba_2YOsO_6 has the ideal cubic double perovskite structure $Fm\bar{3}m$ to within experimental measurement limits; see Supplemental Material [19] for high-resolution synchrotron x-ray and neutron diffraction.

The RIXS measurements reported here reveal the dramatic splitting of the t_{2g} manifold. Using an intermediate coupling approach, we show that this splitting arises due to strong SOC and that the electronic ground state is a spin-orbit entangled $J = 3/2$ state. These results provide a natural explanation of the strong SOC effects observed in $5d^3$ systems [5–9] and further demonstrate that $5d^3$ systems are a platform from which the search for new spin-orbit controlled phases of matter can be pursued. Our work also shows that an intermediate coupling approach is useful
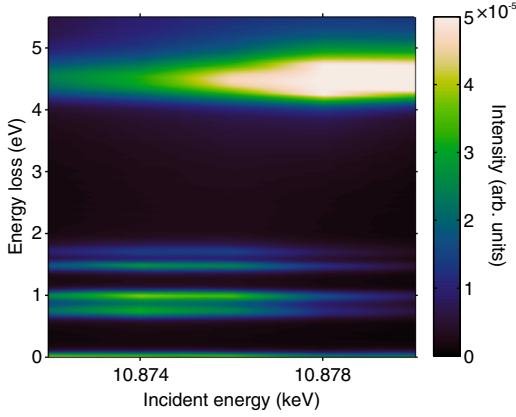
FIG. 1. Incident energy dependence of electronic excitations in Ca_3LiOsO_6. Measurements were performed at 300 K.

to extract the values of spin-orbit and Hund's coupling in cases where the $5d$ transition metal ions are sufficiently isolated, as is the case in many double perovskite and other $5d$-based TMO structure types.

The details of sample synthesis and characterization are provided in the Supplemental Material [19]. RIXS measurements were performed at the Advanced Photon Source (APS) at Sector 27 using the MERIX instrumentation [27]. A closed-cycle refrigerator was used to control the sample temperature. The Os L_3-edge incident energy was accessed with a primary diamond(111) monochromator and a secondary Si(400) monochromator. A Si(466) diced analyzer was used to determine the energy of the beam scattered from the sample, and a MYTHEN strip detector was utilized. All measurements were performed with $2\theta = 90°$ in horizontal geometry. The RIXS energy resolution was 150 meV FWHM. The raw data counts are normalized to the incident beam intensity via an ion chamber monitor. To compare the temperatures, the 6 K data are normalized so that the featureless energy gain side overlaps with the 300 K data—this accounts for deviations of the beam position on the sample.

Figure 1 presents the x-ray energy loss E versus incident energy E_i RIXS spectra of Ca_3LiOsO_6 at 300 K. Four lines are present at $E < 2$ eV, which are enhanced at $E_i = 10.874$ keV, whereas the feature at $E \approx 4.5$ eV is enhanced at $E_i = 10.878$ keV. This indicates that the $E < 2$ eV features are intra-t_{2g} excitations, whereas the higher energy feature is from t_{2g} to e_g excited states, as has been observed in many $5d$ oxides [7,28–30]. Subsequent measurements were optimized to probe the t_{2g} excitations by fixing $E_i = 10.874$ keV.

Figure 2 presents the detailed RIXS spectra of Ca_3LiOsO_6 and Ba_2YOsO_6 at temperatures of 300 and 6 K. In each spectrum there are five peaks in addition to the elastic line: four peaks with $E < 2$ eV, labeled a, b, c, and d [Figs. 2(c) and 2(d)], which we associated with intra-t_{2g} excitations, and a broad peak, e, centered at $E \sim 4.5$ eV

[Figs. 2(a) and 2(b)] associated with t_{2g} to e_g excited states. The size of the splitting is significant and is larger than the splitting between the $J_{eff} = 3/2$ and $J_{eff} = 1/2$ in Sr_2IrO_4 [31]. The qualitative similarity of the spectra of Ca_3LiOsO_6 and Ba_2YOsO_6 indicates that these features are not controlled by noncubic structural distortions, as splittings would be heightened in Ca_3LiOsO_6.

The four t_{2g}-character peaks we observe are incompatible with the multiplets expected in standard crystal field theory developed for $3d$ ions, which leads to the $S = 3/2$ ground state [4]. Here, we identify that a method first proposed by Kamimura *et al.* [32] (see also Ref. [33]) for transition metal halides is relevant in this case, in which the assumption that interelectron interaction energies (including intra- and interorbital Coulomb and exchange interactions) are much larger than SOC is dropped. This approach can be utilized to model our TMO RIXS data, with the primary assumption that the hybridization with the surrounding oxygen ligands leaves the transformation properties of the free ion wave functions unaltered. This, therefore, promotes the breaking of the $S = 3/2$ singlet and strong entry of SOC. The wave functions are therefore described in terms of irreducible representations in the O double group determined by the octahedral symmetry [4,34,35]; see Fig. 3. This formulation does not necessitate approximations that the cubic crystal field is infinite or that Coulomb or SOC must be neglected, and is not restricted to use for $5d^3$ configurations [32].

Before preceding to a more quantitative analysis of the four t_{2g}-character peaks, we briefly discuss the temperature dependence of the RIXS spectrum. At 300 K the peaks a–d are resolution limited, as determined from least-squares fitting of Gaussian peaks on a flat background to the data; see Figs. 2(c) and 2(d). The peak energies for Ca_3LiOsO_6 are $a_{Ca} = 0.760(7)$ eV, $b_{Ca} = 0.992(5)$ eV, $c_{Ca} = 1.470(5)$ eV, and $d_{Ca} = 1.72(1)$ eV, and for Ba_2YOsO_6 are $a_{Ba} = 0.745(7)$ eV, $b_{Ba} = 0.971(7)$ eV, $c_{Ba} = 1.447(9)$ eV, and $d_{Ba} = 1.68(1)$ eV. At 6 K, well below T_N in both materials, the peaks appear broadened, although they maintain the SOC-induced four peak character, indicating that magnetic order is not responsible for splitting of the t_{2g} manifold. The low temperature broadening is most pronounced in peak e—this peak is due to 20 different excited levels in the Coulomb plus SOC regime, so no discrete levels can be resolved with current RIXS capabilities. The broadening could be due to splittings from noncubic structural distortions occurring below the magnetic ordering temperatures—some distortion should be expected from magnetoelastic coupling. However, if a purely structural distortion were the origin we would expect to see broadening in Ca_3LiOsO_6 compared to Ba_2YOsO_6 at all temperatures. It is possible that at low temperatures there is dispersion of the levels [17], or that increased hybridization influences the accessible distribution of excited states—this would be more pronounced for e_g levels which
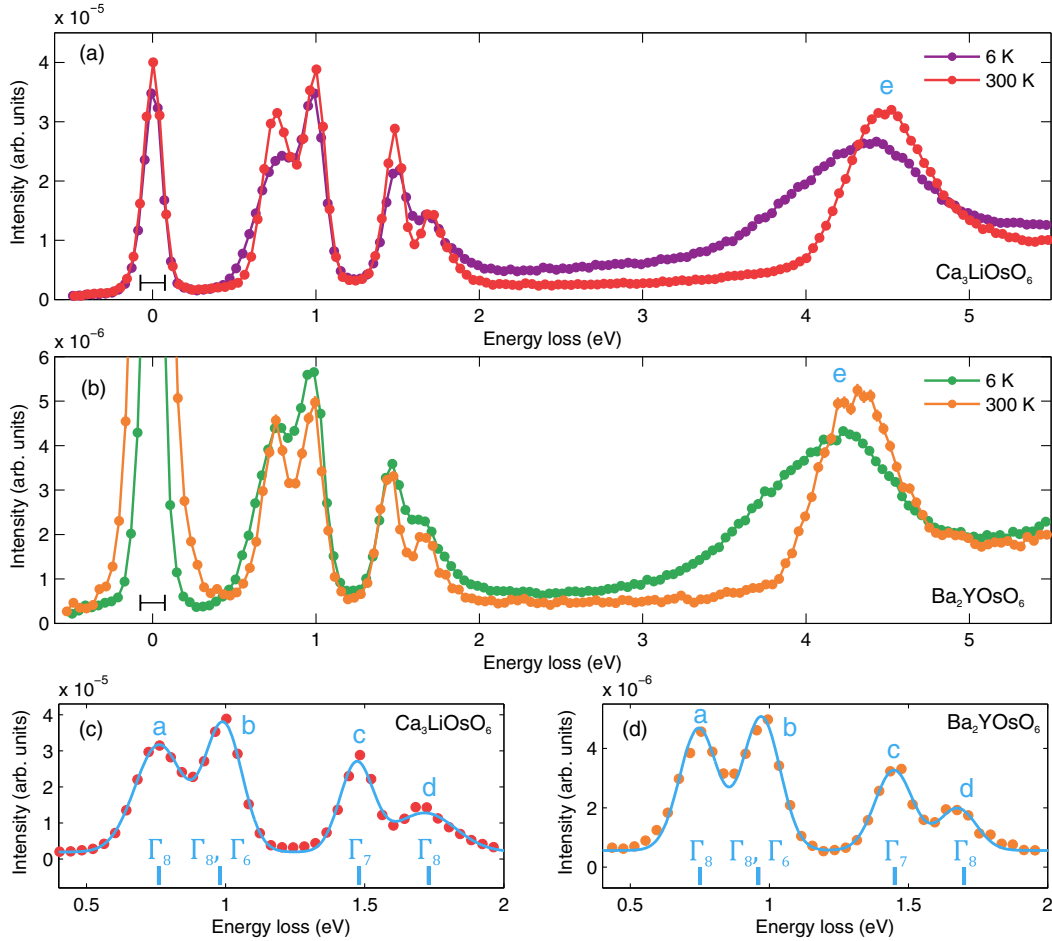
FIG. 2.   RIXS excitation spectra measured in Ca_3LiOsO_6 and Ba_2YOsO_6. Panels (a) and (b) show the data for Ca_3LiOsO_6 and Ba_2YOsO_6, respectively. Black lines indicate the FWHM of the elastic line. Panels (c) and (d) show the energy range 0.4–2 eV, i.e. the t_{2g} manifold, with the results of Gaussian peak fitting to the data shown as solid lines.

show greater oxygen overlap. Here, we focus on what the splitting of the t_{2g}-character peaks reveals about the electronic ground state.

To determine the wave functions for the $5d^3$ case, as in crystal field theory we use initial basis states that describe the ways in which three electrons can occupy the pure t_{2g} and e_g levels (i.e., terms such as $^4A_{2g}$, which is one electron in each of d_{xy}, d_{yz}, d_{xz} with total spin 3/2), and then apply interelectron interaction and SOC between these states. The interelectron interactions are expressed in terms of the Racah parameters B and C. Because of hybridization, the radial form of the d levels are unknown; i.e., B and C deviate from pure ionic values, but the Racah parameters are formulated such that they can be easily extracted from experiment [4,35,36]. The same interactions can be expressed in terms of intra- and interorbital Coulomb interactions U and U' and the effective Hund's coupling J_h, which have the relationships to the Racah parameters $J_h = 3B + C$, $U = A + 4B + 3C$, and $U' = A - 2B + C$ [36]. The Racah parameter A, however, only appears in the diagonal matrix elements of the interactions matrices

and causes a constant shift in all eigenvalues, including the ground state [34,37], so it cannot be determined by the energies of the excited states probed by RIXS. The full interaction matrices are given in Ref. [34]. By numerically diagonalizing the matrices we determine the eigenstates illustrated in Fig. 3, and are able to fit the resulting eigenvalues to the determined energies a_{Ba}–d_{Ba} and a_{Ca}–d_{Ca}, Fig. 2; see Supplemental Material for further details [19]. We fix the value of the crystal field to the peak value of peak e, 10 Dq = 4.5 eV for Ca_3LiOsO_6 and 10 Dq = 4.3 eV for Ba_2YOsO_6, because the positions of levels a–d are insensitive to small changes in this term, and the resulting levels include negligible mixing of e_g states, as expected for a strong cubic crystal field splitting. We note that quantitative comparisons between the measured intensity and calculation are difficult due to the complexity of the RIXS cross section and, consequently, will be left as the subject of future work.

The resulting parameters provide direct insight into the dominant interactions in the materials. For Ca_3LiOsO_6 we find $\zeta_{SOC} = 0.35(7)$ eV, $B = 0.00(5)$ eV, $C = 0.3(2)$ eV,
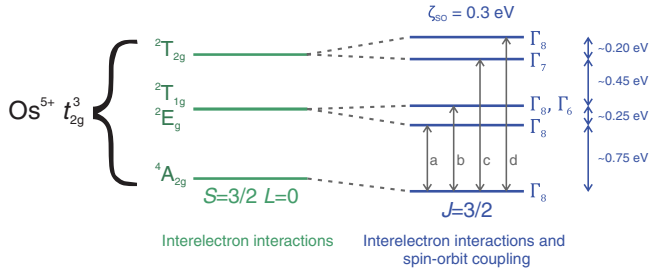
FIG. 3. Structure of t_{2g}^3 levels for Os^{5+} ions in octahedral environment with strong spin-orbit interaction. The irreducible representations for the states without SOC, i.e., $\zeta_{SO} = 0$, are labeled by the appropriate Mulliken symbols; full spatial forms are tabulated in many textbooks, e.g., Ref. [4]. Here, ^2E_g and $^2T_{1g}$ appear degenerate as we determine $B = 0.00(4)$ eV within resolution; see main text. The irreducible representations describing the SOC-induced states are fourfold degenerate, Γ_8, and twofold degenerate, Γ_6 and Γ_7. Dashed lines link the final states with the $\zeta_{SO} = 0$ states that provide the greatest contribution to them; however, each final state is an intermixing of all $\zeta_{SO} = 0$ states, which allows SOC to enter the ground state Γ_8. The labels a, b, c, and d indicate the excited-state energies that are observed in the RIXS spectra of Ba_2YOsO_6 and Ca_3LiOsO_6.

and $J_h = 3B + C = 0.3(2)$ eV, and for Ba_2YOsO_6 we find $\zeta_{SO} = 0.32(6)$ eV, $B = 0.00(5)$ eV, $C = 0.3(2)$ eV, and $J_h = 0.3(2)$ eV. The energy levels calculated for these parameters are given in the Supplemental Material [19]. The fact that ζ_{SO} is of similar size to C (and J_h) clearly demonstrates that perturbative approaches are not appropriate for the treatment of SOC in $5d^3$ systems. The ratio of C/B is commonly used to indicate the scale of deviation from pure ionic wave functions (the nephelauxetic effect) by comparison to the same ratio in $3d$ materials where SOC is weak, with $C/B = 4$ for Cr^{3+} ($3d^3$) ions [4,35]. We find B to be zero within the error, indicative of a large nephelauxetic effect; improved resolution of RIXS measurements would be advantageous for this comparison. We can, however, look at the eigenvector we determined for the Γ_8 ground state— which is a linear combination of the 21 initial basis states which describe 3 electrons occupying the t_{2g} levels, or two occupying the t_{2g} levels and one in the e_g levels (the latter ultimately form a negligible contribution; see Supplemental Material [19]). The largest component is, as expected, from the $S = 3/2$ $|^4A_2\rangle$ state, but the next major contribution is from the $S = 1/2$ $|^2T_{2g}\rangle$ state. For Ca_3LiOsO_6 (Ba_2YOsO_6), these $|^4A_2\rangle$ and $|^2T_{2g}\rangle$ terms appear in the normalized eigenvector with weights of 0.95 (0.95) and 0.27 (0.25), respectively—the complete eigenfunctions are given in the Supplemental Material [19]. This latter component (plus smaller terms) directly explains the entry of SOC physics and the observations of small orbital moments for $5d^3$ ions [5,6,8,9,38].

We finally explore how the framework presented provides insight about the physical manifestation of SOC.

An x-ray absorption near-edge spectroscopy plus x-ray circular dichroism study of $5d^3$ Ir^{6+} double perovskites found strong coupling between orbital and spin moments despite small orbital moments, and suggested this should be due to some deviation from the pure t_{2g}^3 levels [8], with similar results reported in Os^{5+} materials [9]. The wave function we determine explains these results, with a $J = 3/2$ state which has only a small orbital moment. The observation of a large spin gap in the magnetic excitation spectra of Ba_2YOsO_6 and related double perovskites is also explained by the intermediate coupling framework, as the spin gap results from strong SOC-induced anisotropy which is unexplained in a $S = 3/2$ picture. In these double perovskites and the pyrochlore $Cd_2Os_2O_7$ anisotropy is held responsible for stabilization of the observed magnetic ground states [6,7,39]. Furthermore, recent observations of a large spin gap in $NaOsO_3$ [18] and recent theoretical calculations [40] indicate the importance of strong SOC. Finally, the energy scale of the overall spitting of the t_{2g} manifold observed here and the broad intra t_{2g} feature observed in the RIXS spectra of $NaOsO_3$ [18] and $Cd_2Os_2O_7$ [7] is similar, suggesting SOC of a comparable magnitude (see Fig. S4 in Ref. [19]). Our results therefore show that intermediate coupling electronic ground states are influential in dictating the macroscopic physical properties of a broad class of materials. Along these lines, similar studies of $4d^3$ Ba_2YRuO_6 will likely yield deeper insight into the prominence of spin-orbit coupling physics in d^3 systems. We further speculate that a similar approach should be utilized for $5d^2$ and $5d^4$ materials, as they are expected to show larger SOC effects [41], alongside increased hybridization in the d^2 case. The d^4 materials have attracted interest for hosting correlated magnetic moments [42,43] despite the d^4 configuration leading to nonmagnetic singlets in either LS or jj limits [41].

---

[*] christiansad@ornl.gov

[1] G. Jackeli and G. Khaliullin, Phys. Rev. Lett. **102**, 017205 (2009).

[2] W. Witczak-Krempa, G. Chen, Y. B. Kim, and L. Balents, Annu. Rev. Condens. Matter Phys. **5**, 57 (2014).

[3] B. J. Kim, H. Ohsumi, T. Komesu, S. Sakai, T. Morita, H. Takagi, and T. Arima, Science **323**, 1329 (2009).

[4] S. Sugano, Y. Tanabe, and H. Kamimura, *Multiplets of Transition-Metal Ions in Crystals* (Academic Press, New York, 1970).

[5] E. Kermarrec, C. A. Marjerrison, C. M. Thompson, D. D. Maharaj, K. Levin, S. Kroeker, G. E. Granroth, R. Flacau, Z. Yamani, J. E. Greedan, and B. D. Gaulin, Phys. Rev. B **91**, 075133 (2015).

[6] A. E. Taylor, R. Morrow, R. S. Fishman, S. Calder, A. I. Kolesnikov, M. D. Lumsden, P. M. Woodward, and A. D. Christianson, Phys. Rev. B **93**, 220408 (2016).

[7] S. Calder, J. G. Vale, N. A. Bogdanov, X. Liu, C. Donnerer, M. H. Upton, D. Casa, A. H. Said, M. D. Lumsden, Z. Zhao, J.-Q. Yan, D. Mandrus, S. Nishimoto, J. van den Brink, J. P. Hill, D. F. McMorrow, and A. D. Christianson, Nat. Commun. **7**, 11651 (2016).

[8] M. A. Laguna-Marco, P. Kayser, J. A. Alonso, M. J. Martínez-Lope, M. van Veenendaal, Y. Choi, and D. Haskel, Phys. Rev. B **91**, 214433 (2015).

[9] L. S. I. Veiga, G. Fabbris, M. van Veenendaal, N. M. Souza-Neto, H. L. Feng, K. Yamaura, and D. Haskel, Phys. Rev. B **91**, 235135 (2015).

[10] Y. Shi, Y. Guo, S. Yu, M. Arai, A. Sato, A. A. Belik, K. Yamaura, and E. Takayama-Muromachi, J. Am. Chem. Soc. **132**, 8474 (2010).

[11] G. J. Thorogood, M. Avdeev, M. L. Carter, B. J. Kennedy, J. Ting, and K. S. Wallwork, Dalton Trans. **40**, 7228 (2011).

[12] E. E. Rodriguez, F. Poineau, A. Llobet, B. J. Kennedy, M. Avdeev, G. J. Thorogood, M. L. Carter, R. Seshadri, D. J. Singh, and A. K. Cheetham, Phys. Rev. Lett. **106**, 067201 (2011).

[13] Y. Krockenberger, K. Mogare, M. Reehuis, M. Tovar, M. Jansen, G. Vaitheeswaran, V. Kanchana, F. Bultmark, A. Delin, F. Wilhelm, A. Rogalev, A. Winkler, and L. Alff, Phys. Rev. B **75**, 020404 (2007).

[14] S. Calder, V. O. Garlea, D. F. McMorrow, M. D. Lumsden, M. B. Stone, J. C. Lang, J.-W. Kim, J. A. Schlueter, Y. G. Shi, K. Yamaura, Y. S. Sun, Y. Tsujimoto, and A. D. Christianson, Phys. Rev. Lett. **108**, 257209 (2012).

[15] O. N. Meetei, O. Erten, M. Randeria, N. Trivedi, and P. Woodward, Phys. Rev. Lett. **110**, 087203 (2013).

[16] S. Calder, M. D. Lumsden, V. O. Garlea, J. W. Kim, Y. G. Shi, H. L. Feng, K. Yamaura, and A. D. Christianson, Phys. Rev. B **86**, 054403 (2012).

[17] L. J. P. Ament, M. van Veenendaal, T. P. Devereaux, J. P. Hill, and J. van den Brink, Rev. Mod. Phys. **83**, 705 (2011).

[18] S. Calder, J. G. Vale, N. Bogdanov, C. Donnerer, D. Pincini, M. Moretti Sala, X. Liu, M. H. Upton, D. Casa, Y. G. Shi, Y. Tsujimoto, K. Yamaura, J. P. Hill, J. van den Brink, D. F. McMorrow, and A. D. Christianson, Phys. Rev. B **95**, 020413 (2017).

[19] See Supplemental Material at http://link.aps.org/supplemental/10.1103/PhysRevLett.118.207202 where we discuss details regarding the sample preparation and characterization, the RIXS measurements, and the fitting procedure and model, and also includes Refs. [20–26].

[20] M. Wakeshima and Y. Hinatsu, Solid State Commun. **136**, 499 (2005).

[21] B. H. Toby, J. Appl. Crystallogr. **34**, 210 (2001).

[22] J. Rodríguez-Carvajal, Physica (Amsterdam) **192B**, 55 (1993).

[23] C. J. Howard, B. J. Kennedy, and P. M. Woodward, Acta Crystallogr. Sect. B **59**, 463 (2003).

[24] J. Kanamori, Prog. Theor. Phys. **30**, 275 (1963).

[25] M. S. Dresselhaus, G. Dresselhaus, and A. Jorio, *Group Theory: Application to the Physics of Condensed Matter* (Springer, Berlin, 2008).

[26] G. F. Koster, J. O. Dimmock, R. G. Wheeler, and H. Statz, *The Properties of the Thirty-Two Point Groups* (MIT Press, Cambridge, MA, 1963).

[27] T. Gog, G. T. Seidler, D. M. Casa, M. H. Upton, J. Kim, S. Stoupin, K. P. Nagle, M. Balasubramanian, R. A. Gordon, T. T. Fister, S. M. Heald, T. Toellner, J. P. Hill, D. S. Coburn, Y.-J. Kim, A. H. Said, E. E. Alp, W. Sturhahn, H. Yavas, C. A. Burns, and H. Sinn, Synchrotron Radiat. News **22**, 12 (2009).

[28] X. Liu, V. M. Katukuri, L. Hozoi, W.-G. Yin, M. P. M. Dean, M. H. Upton, J. Kim, D. Casa, A. Said, T. Gog, T. F. Qi, G. Cao, A. M. Tsvelik, J. van den Brink, and J. P. Hill, Phys. Rev. Lett. **109**, 157401 (2012).

[29] S. Boseggia, R. Springell, H. C. Walker, A. T. Boothroyd, D. Prabhakaran, D. Wermeille, L. Bouchenoire, S. P. Collins, and D. F. McMorrow, Phys. Rev. B **85**, 184432 (2012).

[30] M. M. Sala, K. Ohgushi, A. Al-Zein, Y. Hirata, G. Monaco, and M. Krisch, Phys. Rev. Lett. **112**, 176402 (2014).

[31] J. Kim, D. Casa, M. H. Upton, T. Gog, Y.-J. Kim, J. F. Mitchell, M. van Veenendaal, M. Daghofer, J. van den Brink, G. Khaliullin, and B. J. Kim, Phys. Rev. Lett. **108**, 177003 (2012).

[32] H. Kamimura, S. Koide, H. Sekiyama, and S. Sugano, J. Phys. Soc. Jpn. **15**, 1264 (1960).

[33] H. Matsuura and K. Miyake, J. Phys. Soc. Jpn. **82**, 073703 (2013).

[34] J. C. Eisenstein, J. Chem. Phys. **34**, 1628 (1961).

[35] B. N. Figgis and M. A. Hitchman, in *Ligand Field Theory and Its Applications*, Special Topics in Inorganic Chemistry (Wiley, New York, 2000).

[36] A. Georges, L. d. Medici, and J. Mravlje, Annu. Rev. Condens. Matter Phys. **4**, 137 (2013).

[37] P. B. Dorain and R. G. Wheeler, J. Chem. Phys. **45**, 1172 (1966).

[38] A. E. Taylor, R. Morrow, D. J. Singh, S. Calder, M. D. Lumsden, P. M. Woodward, and A. D. Christianson, Phys. Rev. B **91**, 100406 (2015).

[39] E. V. Kuz'min, S. G. Ovchinnikov, and D. J. Singh, Phys. Rev. B **68**, 024409 (2003).

[40] B. Kim, P. Liu, Z. Ergönenc, A. Toschi, S. Khmelevskyi, and C. Franchini, Phys. Rev. B **94**, 241113 (2016).

[41] G. Chen and L. Balents, Phys. Rev. B **84**, 094420 (2011).

[42] G. Cao, T. F. Qi, L. Li, J. Terzic, S. J. Yuan, L. E. DeLong, G. Murthy, and R. K. Kaul, Phys. Rev. Lett. **112**, 056402 (2014).

[43] T. Dey, A. Maljuk, D. V. Efremov, O. Kataeva, S. Gass, C. G. F. Blum, F. Steckel, D. Gruner, T. Ritschel, A. U. B. Wolter, J. Geck, C. Hess, K. Koepernik, J. van den Brink, S. Wurmehl, and B. Büchner, Phys. Rev. B **93**, 014434 (2016).